Glycolytic Oscillations and Limits on Robust Efficiency

Fiona A. Chandra, *et al.*

Science **333**, 187 (2011);
DOI: 10.1126/science.1200705

Glycolytic Oscillations and Limits on Robust Efficiency

Fiona A. Chandra,[1]* Gentian Buzi,[2] John C. Doyle[2]

Both engineering and evolution are constrained by trade-offs between efficiency and robustness, but theory that formalizes this fact is limited. For a simple two-state model of glycolysis, we explicitly derive analytic equations for hard trade-offs between robustness and efficiency with oscillations as an inevitable side effect. The model describes how the trade-offs arise from individual parameters, including the interplay of feedback control with autocatalysis of network products necessary to power and catalyze intermediate reactions. We then use control theory to prove that the essential features of these hard trade-off "laws" are universal and fundamental, in that they depend minimally on the details of this system and generalize to the robust efficiency of any autocatalytic network. The theory also suggests worst-case conditions that are consistent with initial experiments.

Minimizing waste, resource use, and fragility to perturbations in system components, operation, and environment (*1*) is crucial to the sustainability of systems ranging from cells to engineering infrastructure. Hard limits on computation, prediction, energy conversion, communication, control, and even measurement are at the heart of modern theories of systems in engineering and science (*2*). Unfortunately, lack of coherence among these subjects makes it difficult to explore the trade-offs between these limits, and a more unified theory is needed to understand and design complex systems. Using the well-studied problem of glycolytic oscillation as a case study, we integrate concepts from biochemistry and control theory (*3*, *4*) to explore the hard limits of robust efficiency.

Glycolytic oscillation, in which the concentrations of metabolites fluctuate, has been a classic case for both theoretical and experimental study in control and dynamical systems since the 1960s (*5*–*8*). Numerous mathematical models have been developed, from minimal models (*9*, *10*) to those with extensive mechanistic detail (*11*). Besides being the most studied control system and the most common, glycolysis is also conserved from bacteria to humans and, presumably, has been under intense evolutionary pressure for robust efficiency. Thus, new insights are less likely to be confounded by either gaps in the literature or evolutionary accidents compared with less well studied biological circuitry. Nevertheless, the function of the oscillations, if any, remains a mystery and one we aim to resolve.

The first step is development of the simplest possible model of glycolysis that illustrates the trade-offs caused by autocatalysis. Biologically motivated minimal models of glycolytic oscillations exist, but analysis of robustness and efficiency trade-offs has not received much attention. Such analysis can provide a much deeper understanding of the underlying basis of glycolytic oscillations as well as illustrate universal laws that are broadly applicable.

Minimal model of glycolysis. Glycolysis is a central energy producer in a living cell, consuming glucose to generate adenosine triphosphate (ATP), which is used throughout the cell. The first steps of the reaction require ATP, making it autocatalytic. In early experiments in *Saccharomyces cerevisiae*, investigators observed two synchronized pools of oscillating metabolites (*12*), which suggested that a two-state model incorporating phosphofructokinase (PFK) might capture some aspects of system dynamics, and indeed, such simplified models (*9*, *10*) qualitatively reproduce the experimental behavior. We propose a minimal system with three reactions (Fig. 1A), for which we can identify specific mechanisms both necessary and sufficient for oscillations (Table 1).

$$\dot{x} = \frac{2y^a}{1+y^{2h}} - \frac{2kx}{1+y^{2g}}$$

$$\dot{y} = -q\frac{2y^a}{1+y^{2h}} + (q+1)\frac{2kx}{1+y^{2g}} - (1+\delta)$$

$$\begin{bmatrix}\dot{x}\\ \dot{y}\end{bmatrix} = \underbrace{\begin{bmatrix}1\\ -q\end{bmatrix}\frac{2y^a}{1+y^{2h}}}_{PFK} + \underbrace{\begin{bmatrix}-1\\ (q+1)\end{bmatrix}\frac{2kx}{1+y^{2g}}}_{PK} + \underbrace{\begin{bmatrix}0\\ -(1+\delta)\end{bmatrix}}_{Consumption} \quad (1.1)$$

In the first reaction in Eq. 1.1, PFK consumes q molecules of y (ATP) with allosteric inhibition by ATP. We lump the intermediate metabolites into one variable, x. In the second reaction, pyruvate kinase (PK) produces $q + 1$ molecules of y for a net (normalized) production of one unit, which is consumed in a final reaction modeling the cell's use of ATP. In glycolysis, two ATP molecules are consumed upstream and four are produced downstream, which normalizes to $q = 1$ (each y molecule produces two downstream) with kinetic exponent $a = 1$. To highlight essential trade-offs with the simplest possible analysis, we normalize the concentration such that the unperturbed ($\delta = 0$) steady states are $\bar{y} = 1$ and $\bar{x} = 1/k$ [the system can have one additional steady state, which is unstable when $(1, 1/k)$ is stable]. [See the supporting online material (SOM) part I]. The basal rate of the PFK reaction and the consumption rate have been normalized to 1 (the 2 in the numerator and feedback coefficients of the reactions come from these normalizations). Our results hold for more general systems as discussed below and in SOM, but the analysis is less transparent.

As most research does, we focus on allosteric activation of the enzyme PFK by adenosine monophosphate (AMP) as the main control point of glycolysis. We assume that the total concentration of adenosine phosphates, including adenosine diphosphate (ADP), in the cell $[A_{tot}] = [ATP] + [ADP] + [AMP]$ remains constant, and the activating effects of AMP can be modeled as ATP inhibition. ATP also inhibits PK activity, although this has been largely ignored in most models [except (*13*, *14*)]. We emphasize its importance and model both inhibitions through exponents h and g. We use linearization to focus initially on

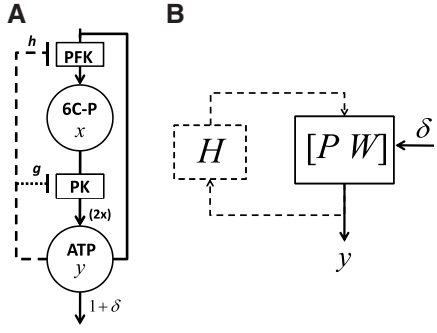

Fig. 1. (**A**) Diagram of two-state glycolysis model. ATP, along with constant glucose input, produce a pool of intermediate metabolites (phosphorylated six-carbon sugars), which then produces two ATPs. ATP inhibits both the first (PFK or PFK-like) and second (PK or PK-like) reactions. (**B**) Control theoretical diagram of the same system (arrows represent logical connections, not fluxes). The system without inhibition or feedback is labeled the "Plant" (P) [solid box, solid and dotted loop in (A)], whereas the inhibitory mechanism is considered the "Controller" (here labeled by its inhibitory strength, *H*) [dashed loop in (A) and (B)]. The effect of disturbance δ in ATP demand is modeled as the system *W* (see text for definition).

[1]Department of Bioengineering, California Institute of Technology, Pasadena, CA 91125, USA. [2]Department of Control and Dynamical Systems, California Institute of Technology, Pasadena, CA 91125, USA.

*To whom correspondence should be addressed. E-mail: fiona@caltech.edu

steady-state error and instability, while highlighting disturbance and control:

$$\begin{bmatrix}\Delta\dot{x}\\ \Delta\dot{y}\end{bmatrix}=\begin{bmatrix}-k & a+g\\ (q+1)k & -qa-g(q+1)\end{bmatrix}\begin{bmatrix}\Delta x\\ \Delta y\end{bmatrix}+\underbrace{\begin{bmatrix}0\\-1\end{bmatrix}\delta}_{Disturbance}+\underbrace{\begin{bmatrix}-1\\q\end{bmatrix}h\Delta y}_{Control} \quad (1.2)$$

The first term on the right-hand side (RHS) gives the dynamics of the "open loop" plant [*P*, defined as Eq. 1.2 when there is no control, i.e., $h = 0$] (solid and dotted loop in Fig. 1A or solid box in Fig. 1B) in response to the second term (disturbance in demand); the third term is the control on PFK (dashed loop in Fig. 1A).

Elementary analysis. The simplest robust performance requirement (motivated by the need to maintain high energy charge) is that the concentration of y remains nearly constant despite fluctuating demand δ. In our model, this requires that the steady-state error ratio be small. This ratio is computed by solving for $|\Delta\bar{y}/\bar{\delta}|$ when

$$\begin{bmatrix}\Delta\dot{x}\\ \Delta\dot{y}\end{bmatrix}=\begin{bmatrix}0\\0\end{bmatrix}$$

$$\text{to be: } \left|\frac{\Delta\bar{y}}{\bar{\delta}}\right|=\left|\frac{1}{h-a}\right| \quad (2.1)$$

This ratio is small when $|h - a|$ is large, and $|\Delta\bar{y}/\bar{\delta}| \to 0$ if and only if $h \to \infty$. One trade-off is that large h requires either high cooperativity or very tight ATP-enzyme binding, and the resulting complex enzymes are more costly for the cell to produce. A more interesting trade-off arises because Eq. 1.2 is stable (see SOM, part II) if and only if

$$0 < h - a < \frac{k+g(1+q)}{q} \quad (2.2)$$

The left-hand side (LHS) bounds the minimum feedback strength h required to stabilize the system, so autocatalysis requires some minimal enzyme complexity for stability, which is compatible with making Eq. 2.1 small. More important, combining Eq. 2.1 and Eq. 2.2 constrains the minimum stable steady-state error to

$$\left|\frac{\Delta\bar{y}}{\bar{\delta}}\right|=\left|\frac{1}{h-a}\right|>\frac{q}{k+g(1+q)} \quad (2.3)$$

Equation 2.3 and Fig. 2A [showing the error bound Eq. 2.3 versus k] illustrate a simple and elegant trade-off between robustness and efficiency (as measured by complexity and metabolic overhead). Low error requires large h, but to allow this to be stable, k and/or g must also be large enough. Large k requires either a more efficient or a higher level of enzymes, and large g requires a more complex allosterically controlled PK enzyme; both would increase the cell's metabolic load. Thus, fragility directly trades off against complexity and high metabolic overhead (low efficiency).

The steady-state error is minimized when h is chosen so that Eq. 2.3 is an equality, but Eq. 1.1 enters sustained oscillations at this hard limit (this boundary is called a supercritical Hopf bifurcation). Thus, at least in this model, oscillations have no direct purpose but are side effects of hard trade-offs crucial to the functioning of the cell and can be avoided at some expense. Note that robustness means making fragility (steady-state error and oscillations) small, and efficiency means making metabolic overhead (enzyme amount and complexity) small.

Hard limits on robust efficiency. Thus far, we have described simple trade-offs based on basic biochemical features of a minimal model. Our elementary analysis of Eq. 1.2 is consistent with existing literature yet clarifies in Eq. 2.3 how oscillations are the inevitable side effect of robust efficiency and trade-offs between steady-state error and stability. An important next step is to expand to a more detailed and comprehensive model and also to extend the analysis to study global nonlinear stability, stochastics, and worst-case disturbances. We have explored such dimensions, and the results are consistent, although often less accessible (most additional modeling details make the trade-offs worse).

A more fundamental direction, however, is to rigorously prove that the trade-offs suggested by Eq. 2.3 are unavoidable regardless of these neglected details, depend only on the basic properties of autocatalytic and control feedbacks, and are unlikely to be either artifacts of model simplifications or "frozen accidents" of evolution (of course, in principle, anything is possible because there is always some gap between models and reality.) Fortunately, control theory has been developed precisely to address such questions in engineering. Unfortunately, although well known to engineers and mathematicians, control theory has not been integrated into other fields. A good background is given in (*4*).

Control theory focuses our attention on a more complete picture of the transient response to dis-

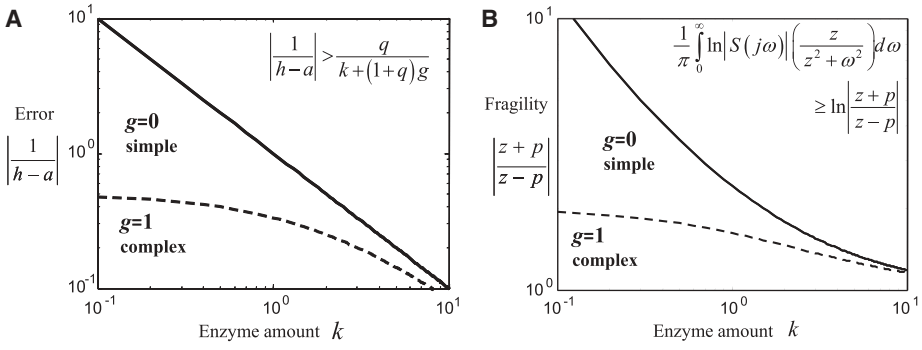

Fig. 2. Trade-offs between waste, fragility, and complexity due to enzyme complexity and amount. Enzyme amount affects the intermediate reaction rate k (x axis), plotted for $g = 0$ (solid line) and $g = 1$ (dashed line). Large k requires high metabolic overhead, and large g requires high enzyme complexity. Even small $g > 0$ enhances the trade-offs, particularly at low k. (**A**) The y axis shows the system's steady-state error, and the curves denote the boundary between stable (above) and oscillatory (below) regions. (**B**) The y axis shows the lower bound of the hard limits in Eqs. 3.4 and 3.6.

Table 1. Description of model variables, parameters, and control theoretic terms.

Model parameters			Definition of terms
x	Lumped variable of intermediate metabolites	$P(s)$	Open loop response ($h = 0$) in frequency (s) domain
y	output, ATP level		
k	Intermediate reaction rate	$WS(s)$	Weighted response to a disturbance δ
δ	Perturbation in ATP consumption		$WS(s) = W(s)S(s)$ where $W(s)$ is the weight
q	Autocatalytic stoichiometry	$S(s)$	Impulse response to a disturbance δ
a	Cooperativity of ATP binding to PFK	z	Zero, the solution to $P(z) = 0$
h	Feedback strength of ATP on PFK	p	Pole, the solution to $W(p) = P(p) = \infty$, or $D(p) = 0$
g	Feedback strength of ATP on PK		

turbances. Because even temporary ATP depletion can induce cell death, large amplitude oscillation can be detrimental (*15*). Therefore, static steady-state response alone provides insufficient information, and the dynamics must be analyzed carefully. To this end, we reconsider the linearized model Eq. 1.2 and allow $\delta = \delta(t)$ to be an arbitrary function of time, although the figures only show responses of the nonlinear system Eq. 1.1 to step changes in $\delta(t)$. The theory is most conveniently written using frequency-domain transforms $\hat{y}(s) \triangleq \int_{-\infty}^{\infty} y(t)e^{-st}dt$, where $s \in \mathbb{C}$ is the (complex) Laplace transform variable, and frequency ω with $s = j\omega$ is the Fourier transform variable. We consider three cases of control: (i) "wild type" with constant h (the case studied above); (ii) a general case where h is replaced by a controller H with arbitrarily complex internal dynamics, constrained only to stabilize Eq. 1.2; and (iii) no control ($h = H = 0$). H is assumed linear and time invariant, and we write $H = H(s)$.

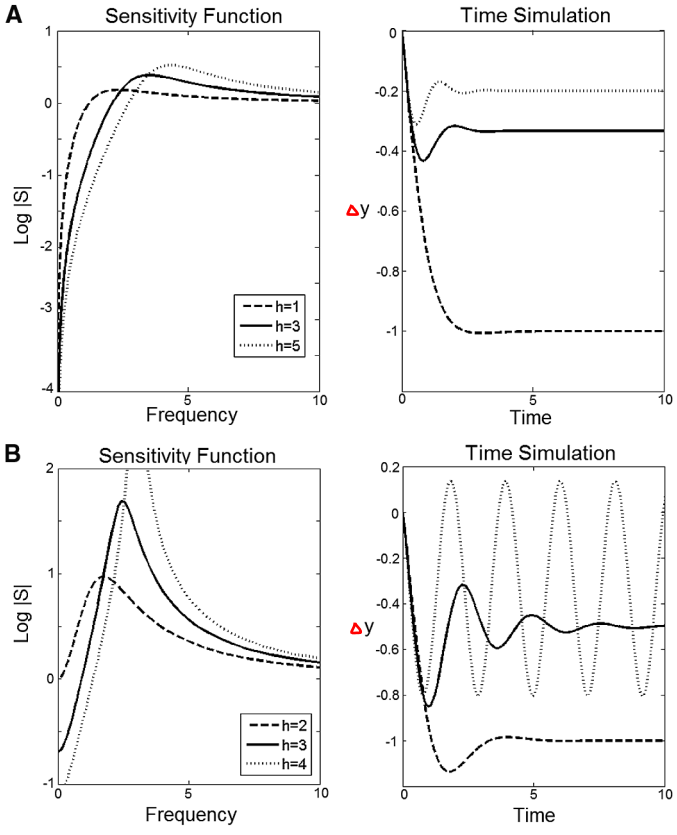

Fig. 3. Log sensitivity $\log|S(j\omega)|$ (left) without ATP feedback on PK ($g = 0$) and step response of the nonlinear system Eq. 1.1 to step change in demand δ (right). The integral of $\log|S(j\omega)|$ is constrained by Eq. 3.5 in (A) (left) and Eq. 3.6 in (B) (left) and is the same for all h. Only the shape changes with increasing h. Higher h gives better steady-state error with more oscillatory transient. (**A**) With no autocatalysis ($q = 0$) the system is stable for all $h > 0$. (**B**) When $q = 1$, $\log|S(j\omega)|$ is more severely constrained by Eq. 3.6 and the system has sustained oscillations for large h.

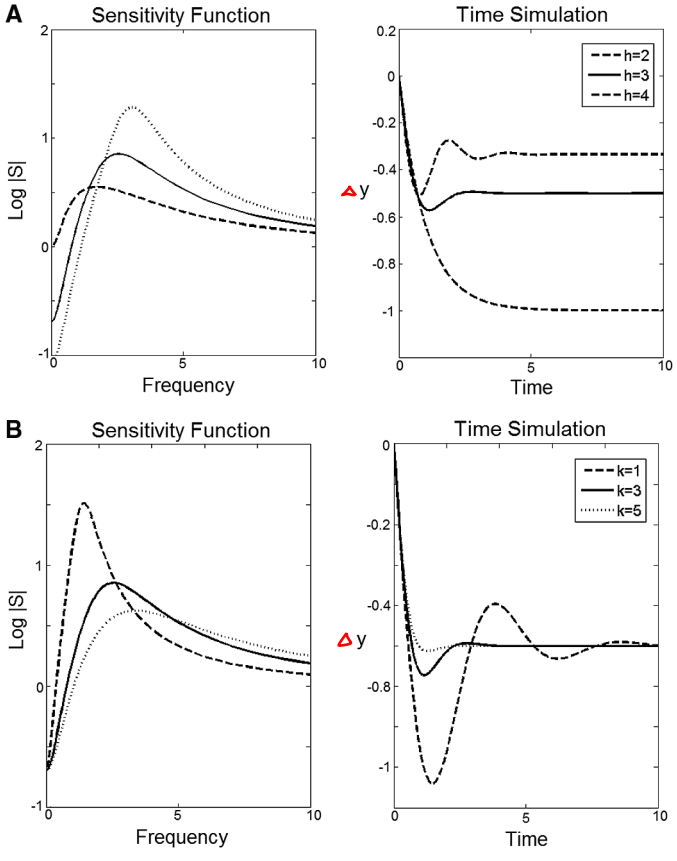

Fig. 4. Log sensitivity $\log|S(j\omega)|$ (left) and step response of the nonlinear system in Eq. 1.1 to step change in demand δ (right). (**A**) The two-state glycolysis model allows higher feedback gain h and better performance when there is an additional feedback loop on PK ($g = 1$). $h = 4$ does not drive the system into sustained oscillation as in the $g = 0$ case in Fig. 3B. Compared with Fig. 3B, both the peaks and total area in $\log|S(j\omega)|$ are lower. (**B**) The effects of varying intermediate reaction rate k given particular inhibition strengths (in this case, $h = 3$ and $g = 1$). Lower k results in both higher peak and area under the curve (left), which translate to more oscillatory transients (right).

The weighted sensitivity transfer function defined as $WS(s) \triangleq \hat{y}(s)/\hat{\delta}(s)$ is the response from δ to y. Given Eq. 1.2 and controller H, we can factor $WS(s) = W(s)S(s)$, where S is called the sensitivity function and W is the weight, equal to the uncontrolled ($H = h = 0$) response from δ to y. For disturbance δ, $W(s)$, $S(s)$, and the open-loop response $P(s)$ (see SOM, part III) are given by

$$W(s) = \frac{s+k}{D(s)}$$

$$S(s) \triangleq \frac{1}{1+P(s)H(s)} = \frac{D(s)}{D(s)+H(s)(-qs+k)}$$

$$P(s) = \frac{-qs+k}{D(s)} \qquad (3.1)$$

where $D(s) = s^2 + [k + g + q(a + g)]s - ka$. With constant, stabilizing $H(s) = h > a$, it follows from Eq. 3.1 and Eq. 2.3 that the response at frequency $\omega = 0$ is equal to the steady-state error ratio:

$$\left|\frac{\Delta\bar{y}}{\bar{\delta}}\right| = |WS(0)| = |W(0)S(0)|$$

$$= \left|\frac{1}{a}\right|\left|\frac{a}{h-a}\right| = \left|\frac{1}{h-a}\right| > \frac{q}{k+g(1+q)} \qquad (3.2)$$

S is the primary robustness measure for feedback control (*3*), and $|S(s = j\omega)|$ measures how much a disturbance is attenuated ($|S(j\omega)| < 1$) or amplified ($|S(j\omega)| > 1$) at frequency ω. $S(s) \equiv 1$ when $H(s) = 0$. The response of y to any other disturbance can be treated with the appropriate weight W.

When there is autocatalysis, we can derive stricter bounds on the response WS and S using the maximum modulus theorem from complex analysis (*16*). In Eq. 3.1, when $q > 0$, $P(s)$ has a zero at $z = k/q$ defined as $P(z) = 0$, which is positive real [$\mathrm{Re}(z) > 0$]. When $a > 0$, both $W(s)$ and $P(s)$ have an unstable pole ($p > 0$), defined as where $W(p) = P(p) = \infty$, and can be computed by solving $D(p) = 0$. So for any stabilizing H: $S(z) = 1$, $S(p) = 0$, and neither $S(s)$ nor $WS(s)$ have poles

in Re(s) ≥ 0. Hence, the maximum modulus theorem holds for $WS(s)$ in the positive real domain Re(s) ≥ 0 (SOM, part III) and

$$\|WS\|_\infty \triangleq \max_{j\omega} |WS(j\omega)| = \max_{\mathrm{Re}(s)\geq 0} |WS(s)| \geq |W(z)S(z)| = \frac{q}{k+qg} \quad (3.3)$$

$$\|S\|_\infty \triangleq \max_{j\omega} |S(j\omega)| = \left\| \frac{s+p}{s-p} S \right\|_\infty \geq \left| \frac{z+p}{z-p} \right| \quad (3.4)$$

The norm $\|WS\|_\infty$ has a variety of interpretations (*3*), the simplest of which is the maximum sinusoidal steady-state response for any frequency ω. Ideally, both WS and S should be low at all frequencies, but this contradicts Eq. 3.3 and Eq. 3.4, which hold regardless of the controller used. The peak $\|WS\|_\infty$ is always larger than the bound in Eq. 3.3 for any h, and minimizing steady-state error $|WS(0)|$ leads to $\|WS\|_\infty \to \infty$ and oscillations (fig. S2). How the RHS of Eq. 3.4 varies with k and g is shown in Fig. 2B; both Eq. 3.3 and Eq. 3.4 are aggravated by small k and g. These are hard constraints on any stabilizing controller from y to the first enzyme, no matter how complex the implementation and, thus, are much deeper than Eq. 2.3, which applies only for constant $H = h$.

Conditions such as those in Eqs. 3.3 and 3.4 can be applied to other transfer functions and weights to provide a rich theoretical framework for exploring additional trade-offs and details, including the realistic frequency content of δ(t), appropriate error penalties in $y(t)$ and other signals, and other sources of noise and uncertainty (*3*, *4*). A complementary focus is on constraints that are independent of these details, such as Bode's integral formula (*3*)

$$\frac{1}{\pi}\int_0^\infty \ln|S(j\omega)|d\omega \geq 0 \quad (3.5)$$

which holds for any linear, stabilizing H that is causal (i.e., H cannot depend on future values of $y(t)$. $H = h$ depends only on current values). This "water bed" effect implies that the net disturbance attenuation ($\ln|S(j\omega)| < 0$) is at least equaled by the net amplification ($\ln|S(j\omega)| > 0$). It is a general constraint on $WS(s)$ for any W, which transparently factors out [$\ln|WS(j\omega)| = \ln|W(j\omega)S(j\omega)| = \ln|W(j\omega)| + \ln|S(j\omega)|$]. For $q = 0$, constant controllers $H = h$ achieve Eq. 3.5 with equality, as illustrated in Fig. 3A. More controller complexity can thus fine-tune the shape of $\ln|S(j\omega)|$ but cannot uniformly improve it. Autocatalysis $q > 0$, however, makes things worse, because $z = k/q$ is finite, and Eq. 3.5 can be strengthened to

$$\frac{1}{\pi}\int_0^\infty \ln|S(j\omega)|\left(\frac{z}{z^2+\omega^2}\right)d\omega \geq \max\left\{0, \ln\left|\frac{z+p}{z-p}\right|\right\} \quad (3.6)$$

with z and p as defined above (for proof, see SOM, part V). It is easily shown that $p > 0$ when $a > 0$ and, otherwise, Eq. 3.6 is just bounded by 0. Hence, autocatalysis always causes positive z and p, and the integral in Eq. 3.6 is bounded similarly to that in Eq. 3.4. The low-pass filter $z/(z^2 + \omega^2)$ constrains the water bed effect to below-frequency $\omega = z$. Small $z = k/q$ produces a more severe limitation, because any disturbance attenuation must be repaid with amplification within a more limited frequency range. The trade-off in three criteria is shown in Fig. 2B: High k both stabilizes the system and reduces the bound but implies high metabolic overhead. How autocatalysis and Eq. 3.6 affect dynamics is illustrated in Fig. 3B. $S(0)$ gives the steady-state error, whereas the peak in $S(j\omega)$ corresponds to how "ringy" the transient $y(t)$ dynamics are at frequency ω. At $h = 2$, $S(0)$ is large, the peak $\|S\|_\infty$ is low, and $y(t)$ has a large steady-state error, which $h = 3$ lowers but with more transient fluctuations. At $h = 4$, the system oscillates at the frequency where $S(j\omega) \to \infty$. Larger q makes z smaller and performance worse (more ringy), as shown in fig. S3. The trade-off in Eq. 2.3 and the difference between Eq. 3.5 and Eq. 3.6 disappears with no autocatalysis ($q \to 0$), because the RHS bound in Eq. 2.3 $\to \infty$ and in Eq. 3.6 $\to 0$. Zero steady-state error with stability is then possible by taking $h \to \infty$.

Complexity and robustness. We have taken PFK feedback as the main controller, but the often neglected PK feedback increases enzyme complexity and plays an important, but subtle, role in robustness. Put most simply, increasing g uniformly improves the stability bound in Eq. 2.3. From Eq. 2.2, if $q = a = 1$, then the system is stable for all $k > 0$ if and only if $0 < h - 1 < 2g$. Thus $g > 0$ is necessary to simultaneously maintain acceptable steady-state error $S(0) = 1/(h - 1)$ and stability for all $k > 0$. Replacing $g = 0$ (Fig. 3B) with $g = 1$ (Fig. 4A) does not change $S(0)$, but $y(t)$ is more damped (and the peaks and integral in Eq. 3.6 are lower). The $h = 4$ case is unstable in Fig. 3B but stable in Fig. 4A. The effect of $g > 0$ on the robustness versus efficiency trade-off involving k gives us insight into how the system is designed. Although a and q are essentially fixed by the network's autocatalytic structure, h and g can be tuned on evolutionary time scales. Thus, $0 < h - 1 < 2g$ is biologically plausible and, in fact, is consistent with most estimates, which ensures stability for all $k > 0$ (*13*). This allows individual cells to further fine-tune $k > 0$ through the many mechanisms that control enzyme levels, but stability for all $k > 0$ also provides robustness to unavoidable noise in gene expression and enzyme levels (*17*). Quantifying this effect would require more detailed modeling and integration of our hard limits on robustness to external disturbances with those in (*17*) on robustness to internal noise in transcription.

From an engineering perspective, this is a remarkably clever control architecture, and the presence of $g > 0$ suggests that, at least in this case, evolution favors higher complexity in exchange for flexibility in k and robustness. Further insights come from the bound in Eq. 3.6. Because $z = k/q$, increasing k improves both sides of Eq. 3.6 and uniformly improves robustness (Fig. 4B), at the expense of higher enzyme levels. Increasing g decreases p, while leaving z unchanged (the dependency of p on g is given in equation S3.9), decreasing $\ln|(z + p)/(z - p)|$ (Fig. 2B). This improves the constraint in Eq. 3.6 and enables more aggressive controller gains h on PFK. By itself (when $h < a$), however, $g > 0$ cannot stabilize, and a stabilizing $G(s)$ needs very high complexity (see SOM, part VI).

Our simple model thus far restricts the controller implementation to ATP inhibition, but other intermediate metabolites can also have inhibitory effects. We show in SOM, part VIII, that control

Table 2. Summary of the performance, metabolic overhead, and stability trade-offs in glycolysis. Each parameter in the two-state model presents its own set of trade-offs.

Parameter	Pros	Cons
Low q	Improves performance limit Can stabilize the system	Reduces metabolic efficiency
High k	Improves performance limit Can stabilize the system	Increases enzyme complexity Increases metabolic load
High h	Stabilizes the system Improves steady-state error	Increases enzyme complexity High h can lead into a limit cycle Worsens transient oscillations
Additional feedback loop ($g > 0$)	Improves performance limit Improves stability bounds	Increases pathway complexity Increases enzyme complexity

by intermediate metabolites can relax stability and performance constraints at the cost of lower efficiency. Intermediate inhibition on PFK can change both the steady-state error and stability bounds, whereas intermediate activation of PK can lift performance constraint (ultimately, the effects of both are limited by enzyme saturation). Fructose 1,6-bisphosphate (the product of PFK) has been thought to both inhibit PFK and activate PK, which also suggests that nature accepts greater complexity in return for robustness.

Experiments revisited. Our theory shows both how autocatalysis makes glycolysis more prone to sustained oscillations and how sufficiently complex feedback control ameliorates this potential fragility. The trade-offs summarized in Table 2 suggest that ringy transient dynamics would be more likely under specific worst-case conditions that we have attempted to create experimentally. Small $z = k/q$ has the most obvious impact on overall fragility, and this occurs at high autocatalytic stoichiometry q and/or low k. Thus, to get a worst-case high-q and low-k condition, wild-type *S. cerevisiae* cells (strain W303) were first grown in ethanol and briefly starved in phosphate-buffered saline, then rapidly shifted into anaerobic glucose metabolism (*18*). Transcription levels of some glycolytic genes are decreased when *S. cerevisiae* is grown in ethanol (*19*), which could decrease k. Flow cytometry of fluorescence-tagged proteins indeed shows lower concentrations of glycolytic enzymes involved in the intermediate reactions in cells grown in ethanol compared with glucose (*18*).

Our single-cell autofluorescence measurements of the reduced form of nicotinamide adenine dinucleotide (NADH) showed that a portion of the cells indeed exhibited fluctuating transients before settling into a higher NADH level (fig. S6), as expected from a robust controller and roughly corresponds to $1 \leq k \leq 3$ in Fig. 4B (right). The period is in good agreement with the 36-s period in cell suspensions (*20*), and this transient does not occur in cells grown in glucose (fig. S7), also as expected for high k [e.g., $k = 5$ in Fig. 4B (right)]. We observe no sustained oscillation regardless of the experimental perturbations applied, which suggests that the intact single cell is indeed rather robust.

In fact, despite intense experimental study, spontaneous sustained oscillations in yeast have only been observed in cell-free extracts or in intact cells in dense suspensions but not when isolated (*20*). Our single-cell model is too simplistic to be as predictive as the detailed models in the literature, but because the analysis highlights fundamental trade-offs, it can give insights into these different behaviors. For example, in cell-free extracts, parameters can be pushed into regimes exposing extreme fragilities that wild-type cells have evolved to avoid. In SOM, part X, we show that our model and theory are consistent with observed patterns of oscillations in well-known extract experiments (*5*). Of course, the possibility of single-cell oscillation cannot be ruled out, and there is much more to be done theoretically and experimentally to fully resolve this. The tools and analysis presented here can be applied to more complete models and, it is hoped, can clarify future directions. In SOM, part XI, we further discuss what is needed to address both dense cell suspensions and isolated cells.

Discussion. Our analysis illustrates the power of control theory to clarify biological phenomena and biology so as to motivate new theoretical directions (*21*). In this simple model of glycolysis, oscillation is neither directly purposeful nor an evolutionary accident but a necessary consequence of autocatalysis and hard trade-offs between robustness and efficiency (or fragility and overhead). Nature has evolved a control structure finely tuned to effectively manage these trade-offs with flexibility to adapt to changes in supply and demand, at the cost of higher enzyme complexity. Consistent with engineering, purposeful complexity in biology is primarily driven by robustness, not minimal functionality (*1*), and there are hard trade-offs that this complexity mediates.

The theory presented here is consistent throughout in highlighting hard trade-offs, but there are important differences in the details. Although Eq. 2.3 is phenomenological and specific to the model in Eq. 1.2, the theory in Eqs. 3.3 to 3.6 is more complete, holding for all frequencies and arbitrarily complex causal controllers, and also applying to other systems. However, Eq. 3.6 still requires substantial phenomenology, because the formulas for z and p depend on assumptions about autocatalysis (q and a) and enzyme efficiencies and levels (k). It is hoped that this will encourage efforts in further unification of control theory with thermodynamics and statistical mechanics, and recent progress is encouraging (*22*). It also leads to rethinking how biology overcomes the "causality" limit with various mechanisms that exploit predictable environmental fluctuations (e.g., circadian rhythms) or provide remote sensing (e.g., vision and hearing), both of which can greatly mitigate hard limits such as Eq. 3.6 (*23*). In the case of circadian rhythms, oscillation is not just a side effect but has the purpose of exploiting predictable periodicity in the environment.

Although our minimal model has limited quantitative predictive power, it can still provide qualitative insights about experiments, such as which parameters to perturb and why extracts oscillate more easily than isolated cells (SOM, parts X and XI). To maximize accessibility, we used the simplest possible model that captures the real system's essential features, yet facilitates theoretical analysis connecting network structure with functional trade-offs and allows the results to be carried out analytically [a model's scope and fidelity versus ease of theoretical analysis is itself an inherent trade-off (*24*)]. The SOM covers various extensions to our model, including a nonlinear model of arbitrary length (SOM, part XII) (*25*) and reversible reactions (SOM, part XIII). The effect of reversibility in the intermediate (PK) reaction depends on PK inhibition strength g and can either ameliorate performance limit at the cost of efficiency, or make it worse. The analysis readily scales to more complex models with appropriate computer-aided design software, but the results are far less accessible.

This research article ultimately raises more questions than it answers, and there is much more to be done experimentally and theoretically. Tuning the autocatalytic and control feedbacks via enzyme mutations to affect robustness is an interesting direction for future experiments. A relatively easy theoretical direction that is largely unexplored is to generalize the bounds in Eqs. 3.3 and 3.4 to complex multivariable feedback systems involving more enzymes and metabolites. Control of additional complex autocatalytic processes, such as redox balance and biosynthesis of building blocks and enzymes, is crucial for a more complete understanding. For example, without aerobic metabolism, NADH is no longer an energy source but a waste product that must be reduced to nicotinamide adenine dinucleotide via other cellular mechanisms, and then recycled, a potentially destabilizing autocatalytic loop. The hard limits can also be generalized to nonlinear systems and controllers with more complex definitions and proofs, but many questions remain open (see SOM, part XV, and references therein). Finally, autocatalytic recycling and control feedbacks must increase and work together effectively in all human systems as we seek to be more sustainable, efficient, and robust.

References and Notes

1. M. E. Csete, J. C. Doyle, *Science* **295**, 1664 (2002).
2. These limits are associated with names such as Turing, Gödel, Poincaré, Carnot, Shannon, Bode, Wiener, and Heisenberg and are the foundation for subjects with a vast literature, including textbooks and popular expositions. Unfortunately, integrated treatments are surprisingly lacking. For a recent survey of some dimensions of this problem, see (*26*).
3. J. C. Doyle, B. A. Francis, A. Tannenbaum, *Feedback Control Theory* (Macmillan, New York, 1992).
4. K. Astrom, R. M. Murray, *Feedback Systems: An Introduction for Scientists and Engineers* (Princeton Univ. Press, Princeton, NJ, 2008).
5. A. Ghosh, B. Chance, *Biochem. Biophys. Res. Commun.* **16**, 174 (1964).
6. P. Richard, *FEMS Microbiol. Rev.* **27**, 547 (2003).
7. B. Teusink, B. M. Bakker, H. V. Westerhoff, *Biochim. Biophys. Acta* **1275**, 204 (1996).
8. M. Bier, B. Teusink, B. N. Kholodenko, H. V. Westerhoff, *Biophys. Chem.* **62**, 15 (1996).
9. A. Goldbeter, *Biochemical Oscillations and Cellular Rhythms* (Cambridge Univ. Press, Cambridge, 1996).
10. E. E. Sel'kov, *Eur. J. Biochem.* **59**, 151 (1975).
11. F. Hynne, S. Danø, P. G. Sørensen, *Biophys. Chem.* **94**, 121 (2001).
12. A. Betz, B. Chance, *Arch. Biochem. Biophys.* **109**, 585 (1965).
13. Y. Termonia, J. Ross, *Proc. Natl. Acad. Sci. U.S.A.* **78**, 2952 (1981).
14. P. H. Richter, J. Ross, *Science* **211**, 715 (1981).
15. B. V. Chernyak, O. Y. Pletjushkina, D. S. Izyumov, K. G. Lyamzaev, A. V. Avetisyan, *Biochemistry* (*Moscow*) **70**, 240 (2005).
16. The maximum modulus theorem applied to rational functions, such as $WS(s)$, says that on any domain in the complex plane that contains no poles of $WS(s)$, the

maximum modulus |*WS*(*s*)| is always achieved on the boundary. See (*3*).
17. I. Lestas, G. Vinnicombe, J. Paulsson, *Nature* **467**, 174 (2010).
18. Materials and methods are available as supporting material on *Science* Online.
19. A. Ståhlberg *et al*., *BMC Genomics* **9**, 170 (2008).
20. A. K. Poulsen, M. Ø. Petersen, L. F. Olsen, *Biophys. Chem.* **125**, 275 (2007).
21. P. A. Iglesias, B. P. Ingalls, *Control Theory and Systems Biology* (MIT Press, Cambridge, MA. 2010).
22. H. Sandberg, J. C. Delvenne, J. C. Doyle, *IEEE Trans Auto Control*, **56**, 293 (2011).
23. N. C. Martins, M. A. Dahleh, J. C. Doyle, *IEEE Trans. Automat. Contr.* **52**, 56 (2007).
24. A. D. Lander, *PLoS Biol.* **2**, e164 (2004).
25. G. Buzi, U. Topcu, J. Doyle, *Automatica*, **47**, 1123 (2011).
26. D. L. Alderson, J. C. Doyle, *IEEE Trans Syst. Man Cybernet. Part A Syst. Hum.* **40**, 839 (2010).

Acknowledgments: The authors thank H. El-Samad and J. Stewart-Ornstein at the University of California, San Francisco, for their laboratory space and assistance; N. Pierce (Ray Deshaies' lab) for the green fluorescent protein library; O. Venturelli (Richard Murray's lab) for her help; and M. Csete for helpful feedback. Microscopy was performed at the Nikon Imaging Center at UCSF. Experimental data are available in SOM. This work is supported by the NIH (award R01GM078992A) and Institute of Collaborative Biotechnologies from the U.S. Army Research Office (subaward KK4102, prime award DAAD19-03-D-0004).

Supporting Online Material
www.sciencemag.org/cgi/content/full/333/6039/187/DC1
Materials and Methods
SOM Text
Figs. S1 to S10
Tables S1 and S23
References (*27*–*31*)

22 November 2010; accepted 2 May 2011
10.1126/science.1200705

The Onset of Turbulence in Pipe Flow

Kerstin Avila,[1]* David Moxey,[2] Alberto de Lozar,[1] Marc Avila,[1] Dwight Barkley,[2,3] Björn Hof[1]*

Shear flows undergo a sudden transition from laminar to turbulent motion as the velocity increases, and the onset of turbulence radically changes transport efficiency and mixing properties. Even for the well-studied case of pipe flow, it has not been possible to determine at what Reynolds number the motion will be either persistently turbulent or ultimately laminar. We show that in pipes, turbulence that is transient at low Reynolds numbers becomes sustained at a distinct critical point. Through extensive experiments and computer simulations, we were able to identify and characterize the processes ultimately responsible for sustaining turbulence. In contrast to the classical Landau-Ruelle-Takens view that turbulence arises from an increase in the temporal complexity of fluid motion, here, spatial proliferation of chaotic domains is the decisive process and intrinsic to the nature of fluid turbulence.

The seemingly simple question as to when the flow down an ordinary pipe turns turbulent dates back to the pioneering study of Osborne Reynolds in the late 19th century (*1*). Reynolds proposed that below a critical velocity, pipe flows are always laminar, whereas above that critical velocity turbulence prevails, given the right initial conditions. The observation that this critical point can be expressed in a dimensionless form was the basis of one of the central concepts in fluid dynamics: the Reynolds number ($Re = UD/\nu$, where U is the mean velocity, D is the pipe diameter, and ν is the kinematic viscosity). Curiously, although Reynolds similarity has proved to be valid throughout fluid mechanics the value of the critical point in pipe flow has been debated ever since. In an early attempt to determine its value (*2*), Reynolds rewrote the equations of motion, separating quantities into average and fluctuating parts—a method that is now called the Reynolds decomposition. This contribution is generally regarded as the foundation of modern turbulence research, but it has failed to clarify the value of the critical point in pipe flow. Values reported in contemporary textbooks and journal papers vary widely, typically ranging from 1700 to 2300 (*3*–*5*), and occasionally even values in excess of 3000 (*6*) are quoted.

One circumstance that complicates this problem is that laminar pipe flow is stable to infinitesimal perturbations (*7*, *8*), and therefore in order to trigger turbulence, a disturbance of finite amplitude is required (*1*, *3*, *9*). What makes matters even more difficult is that at low Re, turbulence is transient. Here, turbulence occurs in the form of localized patches called puffs (*10*) that are embedded in the surrounding laminar flow and decay according to a memoryless process (that is, independent of their previous history) (*11*). The rapid increase in lifetime with Re has led to various proposed values for a critical point at which the lifetime would diverge and turbulence would become sustained (*4*, *12*, *13*). However, more detailed studies (*14*–*18*) have shown that the lifetime of individual puffs remains finite and only approaches infinity asymptotically with Re. Qualitatively, this behavior is reminiscent of the dynamics of a class of model systems called coupled map lattices (*19*). Here, individual lattice points can exhibit transient chaotic dynamics but eventually settle to a stable laminar fixed point. Because of the spatial coupling, these systems exhibit a statistical phase transition as the control parameter is increased. Below the critical point, eventually all sites will end up in the laminar phase, whereas above there is always a nonzero fraction of chaotic sites, and with increasing control parameter the fraction of laminar (nonchaotic) sites quickly diminishes. Analogies to fluid flows have been pointed out in a number of studies (*20*–*23*) that indicate the potential relevance of the spatial dynamics for the long-term behavior in fluid systems. In a numerical study of pipe flow, Moxey and Barkley (*24*) observed that at $Re \approx 2300$ turbulent puffs delocalize, and the turbulent fraction increases, which is in qualitative agreement with this picture. However, the stochastic nature of the spatial coupling was not taken into account, and the extremely long time-scales intrinsic to the flow could not be resolved in the simulations. In this work, we determined the critical point in pipe flow and quantified the relevant process sustaining turbulence in linearly stable shear flows.

Long-pipe experiments. Determining the point at which the proliferation of turbulence outweighs its decay and turbulence eventually becomes sustained requires that the time scales of both decay and spreading processes be captured. Because turbulent puffs move downstream at approximately the mean flow velocity, a long pipe is required to observe long time-scales. Using a precision glass tube with a relatively small diameter ($D = 4 \pm 0.01$ mm) and overall length of 15 m, a total dimensionless length of $3750D$ is achieved. The pipe is composed of 14 sections joined by machined perspex connectors that provide an accurate fit. A smooth inlet together with careful alignment of the individual pipe sections allows the flow to remain laminar up to $Re = 4400$. Deviations in Re were kept below ±5 throughout each set of measurements, which extended over periods of up to 45 hours. This precision was achieved with stringent control of both the pressure difference driving the flow and the fluid (water) temperature (±0.05 K). A detailed description of the experimental setup can be found in (*16*).

Starting from a fully developed laminar flow allows us to induce turbulence in a controlled manner and quantify the spreading rate at some downstream position. The experimental procedure is to create a single turbulent puff close to the pipe inlet and to monitor any changes in the turbulent fraction at downstream positions. It is important that a perturbation is chosen that efficiently triggers turbulence. In many earlier studies, such as (*10*, *25*), turbulence was induced by insertion of a static obstacle close to the pipe inlet. Such obstacles provide a continuous perturbation, and at high Reynolds numbers the flow downstream is fully turbulent, whereas in the transitional

[1]Max Planck Institute for Dynamics and Self-Organization, Bunsenstrasse 10, 37073 Göttingen, Germany. [2]Department of Mathematics, University of Warwick, Coventry CV4 7AL, UK. [3]Physique et Mécanique des Milieux Hétérogènes, UMR 7636 CNRS–École Supérieure de Physique et de Chimie Industrielles de la Ville de Paris–Univ Paris 06–Univ Paris 07, 10 rue Vauquelin, 75005 Paris, France.

*To whom correspondence should be addressed. E-mail: kavila@ds.mpg.de (K.A.); bhof@ds.mpg.de (B.H.)